Annealed Star-Branched Polyelectrolytes in Solution

J. Klein Wolterink,*,† J. van Male,† M. A. Cohen Stuart,† L. K. Koopal,† E. B. Zhulina,‡,⊥ and O. V. Borisov§,⊥

Laboratory for Physical Chemistry and Colloid Science, Wageningen University, 6703 HB Wageningen, The Netherlands; Department of Chemistry and Biochemistry and Center for Polymer Research, The University of Texas at Austin, Austin, Texas 78712; Laboratoire de Recherche sur les Matériaux Polymères, UMR 5067 CNRS UPPA, 64053 Pau, France; and Institute of Macromolecular Compounds of the Russian Academy of Sciences, 199004 St. Petersburg, Russia

Received May 22, 2002; Revised Manuscript Received August 26, 2002

ABSTRACT: Equilibrium conformations of annealed star-branched polyelectrolytes (polyacids) are calculated with a numerical self-consistent-field (SCF) model. From the calculations we obtain also the size and charge of annealed polyelectrolyte stars as a function of the number of arms, pH, and the ionic strength. The results are compared with predictions from analytical theory. Upon varying the number of branches or the ionic strength of the solution, the star size changes nonmonotonically, which is in agreement with the analytical predictions. The salt concentration at this maximum is directly related to the charge density of the star. The internal structural properties of the star corona (the polymer density, the ionization profiles, and the distribution of the end points) are analyzed. The shape of the density profiles indicates increasing local stretching of the branches as a function of the distance from the star center. Furthermore, a bimodal end-point distribution is found and interpreted in analogy to that predicted earlier by analytical SCF theory for planar polyelectrolyte brushes. Results of recent experiments with annealed star-shaped micelles are discussed on the basis of our numerical model calculations.

1. Introduction

Weakly dissociating polyelectrolytes play an important role in stabilizing colloids and in buffering environments.[1] An example is the buffer capacity of soils: weak acidic polyelectrolytes, i.e., humic acids, regulate a change in the pH and/or the (heavy) metal ion concentration. Micelles with a polyelectrolyte corona have practical relevance in drug and pesticide delivery systems.[2]

Solutions of polyelectrolytes, in general, still remain one of the under-explored fields in polymer science since the conventional linear Debye−Hückel approximation usually fails to describe structural properties of the solutions of highly charged polyions. Even though the properties of solutions of linear chain polyelectrolytes are not completely understood, charged polymers of more complex architecture, such as randomly[3] or regularly[4−8] branched polyelectrolytes, have attracted considerable attention.

Polyelectrolyte stars, comprising a relatively small core region and an extended charged corona, resemble polymeric micelles[9−17] or small colloidal particles stabilized by grafted polyelectrolytes. Furthermore, a starlike architecture provides the simplest model of branching and is useful for getting an insight into the behavior of branched polyelectrolytes with more complex architecture.

Two types of polyelectrolytes can be distinguished: quenched (or strong) and annealed (or weak). The dissociation constant for a monomer of a quenched polyelectrolyte is so high that the actual degree of ionization is constant, irrespective of the local electrostatic potential. The number of charges per molecule is a constant irrespective of the system. Poly(styrenesulfonate), PSS, serves as a typical example of a quenched polyelectrolyte. On the other hand, the degree of ionization of an annealed polyelectrolyte depends strongly on the local electrostatic potential because the ionization constant of the monomer is low. The number of charges on an annealed polyelectrolyte will depend on the pH, salt concentration, or polyelectrolyte concentration. Poly(acrylic acid) is a well-known example of an annealed polyelectrolyte.

In our present study we focus on the conformational properties of a weak star-branched polyacid. Making the choice of $pK_{acid} = 5$ for the acidic monomer and assuming a given fraction of acidic monomers in the branches, we thus mimic, e.g., a star-shaped partially hydrolyzed poly(acrylamide) or a star-shaped poly(acrylic acid).

The polyacid stars respond not only to the variation in salt concentration, as in the case of quenched polyelectrolytes, but also to the pH of the solution. The reaction with hydrogen ions is specific and therefore more sensitive to small changes in the concentration of these ions than to the change in concentration of indifferent salt ions.

The most spectacular trends in the large-scale behavior of annealed star-branched polyacids (e.g., the nonmonotonic dependence of the gyration radius upon the number of branches or ionic strength of the solution) were treated earlier on the basis of a scaling approach.[7] In this scaling analysis the local electroneutrality approximation (LEA) is utilized. LEA assumes accumulation of the majority of counterions in the interior of the many-arm polyelectrolyte stars. However, for real polyelectrolyte stars, both simple theoretical estimates and numerical solution of the Poisson−Boltzmann (PB) equation for the distribution of counterions show that a nonnegligible fraction of counterions are released from

† Wageningen University.
‡ The University of Texas at Austin.
§ Laboratoire de Recherche sur les Matériaux Polymères.
⊥ Institute of Macromolecular Compounds of the Russian Academy of Sciences.

10.1021/ma020781j CCC: $22.00
Published on Web 10/25/2002

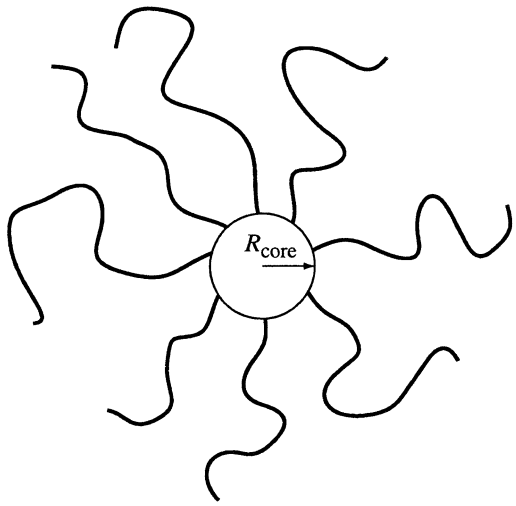

Figure 1. Schematic picture of a star-shaped polyelectrolyte with an impenetrable core.

the corona of the polyelectrolyte. Therefore, to find out whether LEA is justified, a more accurate approach based on the numerical solution of the PB equation is required.

We analyze in a systematic way the effects of branching (number of arms in the star), ionic strength, and pH of the solution on the conformational properties of the annealed star-branched polyelectrolyte. The numerical SCF theory that will be applied here is based on the Scheutjens−Fleer (SF−SCF) algorithm.[18] It is a powerful method for getting an insight into the radial distributions of the polymer and the counterion density in stars or micellar coronae. No a priori assumptions, other than the mean-field approximation and Gaussian chain statistics, are made about the conformations of the polyelectrolyte stars or about the distribution of counterions. Also, a quantitative prediction concerning their scattering behavior can be made. The latter will be compared to recent SANS experiments, which probed the internal structure of the corona of starlike polyelectrolyte micelles.[16]

The paper is organized as follows: In section 2 we present an overview of the results of the analytical theory concerning the behavior of annealed star-branched polyelectrolytes in dilute solutions.[7] This work is extended for the case of arbitrary pH of the solution. In section 3 we give the most important features of the numerical SCF model. Results and discussion are given in section 4. We end up with the comparison of our calculations with a recent experiment (section 5) and with the conclusions in section 6.

2. Analytical Model

The analytical model considers a star-branched polyelectrolyte comprising f branches (arms), attached with one end onto an impermeable core of size R_{core} (Figure 1). The size of the core is assumed to be small with respect to that of the arms, and it will be neglected in the analytical model.

Each arm is a linear, intrinsically flexible polymer chain comprising N monomers. The star consists of fN monomers. Each mth monomer ($m = 1, 2, ...$) is capable of ionization via dissociation of a hydrogen ion H^+. The fraction of ionized acidic monomers at a place r is denoted as $\alpha(r)$ and depends on the local proton volume fraction $\varphi_{H^+}(r)$ as[19]

$$\frac{\alpha(r)}{1-\alpha(r)} = \frac{K}{\varphi_{H^+}(r)} \tag{1}$$

where K is the dissociation constant. By using the local proton volume fraction, we assume in eq 1 that the activity coefficient is 1. The overall charge Q of the star-branched poly ion is given by $Q = \alpha fNe/m$, where e is the elementary charge.

In experimentally relevant situations water is a marginally good solvent for the uncharged monomers. In our analysis we therefore assume θ-solvent conditions for the uncharged monomers.

The properties of polyelectrolyte stars in a dilute salt-free solution depend on the number of branches. Three regimes can be distinguished:[6,7]

(i) The *polyelectrolyte regime* occurs for stars with a small number of branches. In this case most of the counterions are released into the bulk of the solution. The star size is determined by the interplay between electrostatic repulsion and a conformational entropy penalty for the extension of the branches (conformational elasticity).

(ii) The *osmotic regime* occurs for stars with a larger number of branches, which retain most of the counterions in the intrastar space. The size is determined by the interplay between osmotic pressure of counterions and conformational elasticity of the branches.

(iii) The *quasi-neutral regime* appears if the number of branches is further increased. This regime is not dominated by the charge of the polyelectrolyte because the steric interactions are larger. The size is determined by the interplay between steric repulsion between the monomers and conformational elasticity of the branches.

2.1. Polyelectrolyte Regime. For stars with a small number of arms, counterions spread uniformly over the solution. The dissociation of a monomer, which is part of the polyelectrolyte star, is then approximately equal to the dissociation of a monomer in the bulk: $\alpha \approx \alpha_b$. The degree of ionization α_b at zero electrostatic potential obeys the equation

$$\frac{\alpha_b}{1-\alpha_b} = \frac{K}{\varphi_{bH^+}} \tag{2}$$

where φ_{bH^+} is the volume fraction of hydrogen ions in the bulk of the solution; eq 2 is a limiting value of eq 1. Because $\alpha \approx \alpha_b$, it follows that in the polyelectrolyte regime annealed polyelectrolytes at a given pH and quenched polyelectrolytes behave identically. At low salt concentration the star conformation is governed by nonscreened Coulomb repulsion between the arms. The size R of the stars in this regime is given by[7]

$$R \cong Nf^{1/3}\left(\frac{\alpha_b}{m}\right)^{2/3}\left(\frac{l_B}{a}\right)^{1/3} a \tag{3}$$

where $l_B = e^2/\epsilon k_B T$ is the Bjerrum length (ϵ is the dielectric constant of the solvent, k_B is the Boltzmann constant, and T the temperature). The size of the monomer is denoted by a. Because $R \sim N$, the extension of the branches is uniform. In a spherical geometry, this means that the radial distribution of polymer density $\varphi(r)$ in the star is given by

$$\varphi(r) \sim r^{-2} \tag{4}$$

where r is the distance from the center of the star. These relations hold for the case of low or no added salt.

For high salt concentrations, i.e., $\kappa R < 1$ where $\kappa^{-1} = (l_B I_b)^{-1/2}$ is the Debye screening length and I_b is the ionic strength in the bulk and defined as

$$I_b = \frac{1}{2}\sum_i \nu_i^2 \varphi_{bi} \tag{5}$$

where ν_i is the valence and φ_{bi} is, the volume fraction of mobile ions of type i in the bulk. The screened Coulomb interactions inside the polyelectrolyte star can be taken into account via an effective second viral coefficient of monomer/monomer interactions, $v_{eff} \sim (\alpha_b/m)^2 I_b^{-1}$.

The star size and the polymer density distribution are now given by[7]

$$R \cong N^{3/5} f^{1/5} \left(\frac{\alpha_b}{m}\right)^{2/5} I_b^{-1/5} a \tag{6}$$

$$\varphi(r) \sim r^{-4/3} \tag{7}$$

These expressions for the properties of the polyelectrolyte star in solution with added salt are similar to those for a neutral star polymer in a good solvent.[20−22]

2.2. Osmotic Regime. As the number of arms in the star increases, more and more counterions are attracted to the vicinity of the star. With increasing number of arms the fraction of free counterions become asymptotically small.[6,7] For these stars the local electroneutrality approximation (LEA) is applicable even when the solution contains no salt.[6] The LEA assumes local compensation of the immobilized charge on the branches by that of the counterions. In the general case, when in addition to H^+ and OH^- ions the solution contains also salt (e.g., NaCl), the local electroneutrality condition assumes the form

$$\sum_{i^-} \varphi_{i^-}(r) + \alpha(r)\varphi(r)/m = \sum_{i^+} \varphi_{i^+}(r) \tag{8}$$

where $\varphi(r)$ and $\alpha(r)$ are the local volume fraction of the monomers and the local degree of ionization inside the star corona ($R_{core} \le r \le R$); the summation on the rhs is running over all the cationic species (i.e., salt ions $\varphi_{Na^+}(r)$ and hydrogen ions $\varphi_{H^+}(r)$) while the summation on the lhs is running over all the anionic species (i.e., salt ions $\varphi_{Cl^-}(r)$ and hydroxide ions $\varphi_{OH^-}(r)$). To find the local degree of ionization $\alpha(r)$ inside the star, eq 8 has to be combined with eq 1 and to the Donnan rule, which reflects the Boltzmann distribution of co- and counterions between the interior of the star and the bulk of the solution:

$$\varphi_{i^-}(r)/\varphi_{bi^-} = \varphi_{bi^+}/\varphi_{i^+}(r) \tag{9}$$

As a result, one gets an equation that couples the local degree of ionization $\alpha(r)$ to the local polymer concentration $\varphi(r)$:

$$\frac{\alpha(r)}{1-\alpha(r)}\frac{1-\alpha_b}{\alpha_b} = \sqrt{\left(\frac{\alpha(r)\,\varphi(r)}{m\Phi_b}\right)^2 + 1} - \frac{\alpha(r)\,\varphi(r)}{m\Phi_b} \tag{10}$$

where $\Phi_b = \sum_i \varphi_{bi}$, the total volume fraction of all mobile ions in the bulk of the solution; in the case when only monovalent ions are present in the system, $\Phi_b = 2I_b$. In the osmotic regime, the polymer density profile $\varphi(r)$ can be determined by balancing the local osmotic force, $4\pi r^2 \Delta\Pi(r)$, with the elastic force. The elastic force is given by

$$\frac{\mathcal{F}_{elas}}{k_B T} = \frac{3f^2}{4\pi r^2 \varphi(r)} \tag{11}$$

This force is arising in the extended branches.[7] Equation 11 assumes Gaussian elasticity and equal stretching of all the branches. The excess osmotic pressure inside the star is given by

$$\Delta\Pi(r)/k_B T = \sum_i \varphi_i(r) - \Phi_b + \Delta\Pi_\theta(r)/k_B T \tag{12a}$$

$$= \sqrt{(\alpha(r)\varphi(r)/m)^2 + \Phi_b^2} - \Phi_b + \Delta\Pi_\theta(r)/k_B T \tag{12b}$$

where $\Delta\Pi_\theta(r) \sim \varphi^3(r)$ is the contribution due to non-electrostatic (steric) repulsion between the monomers. The latter contribution dominates for the stars with a sufficiently large number of arms and/or close to the center of the star, i.e., when $\varphi(r)$ is sufficiently large while $\alpha(r)$ is small. For the stars that do not have a very large number of arms, the contribution of $\Delta\Pi_\theta(r)$ can be neglected, except for the central region of the star. The behavior of the central part of the star is the same as for a star in the quasi-neutral regime; this will be addressed in section 2.3.

Asymptotic expressions for the size and the polymer density profiles can be obtained in two opposite limits: $\alpha(r)\varphi(r)/m\Phi_b \gg 1$ (osmotic annealing regime) and $\alpha(r)\varphi(r)/m\Phi_b \ll 1$ (salt dominance regime); i.e., the ratio between the local concentration of counterions and the total concentration of mobile ions in the bulk of the solution serves as a natural parameter for expansion of eqs 10 and 12. We remind the reader that Φ_b depends not only on the concentration of added salt but also on the pH of the solution, which in turn determines α_b.

Osmotic Annealing Regime, $\alpha(r)\varphi(r)/m \gg \Phi_b$. This regime occurs when the concentration of added salt is low and while the pH is sufficiently high to induce appreciable ionization of the star arms. Then eq 10 assumes the form

$$\frac{\alpha(r)^2}{1-\alpha(r)} \approx \frac{\alpha_b}{1-\alpha_b}\frac{m\Phi_b}{2\varphi(r)} \tag{13}$$

As one can see from eq 13, the degree of ionization of monomers in the branches $\alpha(r)$ is at low salt concentration much smaller than that in the bulk of the solution α_b, unless $\alpha_b \to 1$, i.e., unless the pH $\gg$ pK.

For this low salt regime, the excess osmotic pressure reduces to

$$\Delta\Pi(r)/k_B T \approx \alpha(r)\varphi(r)/m \tag{14}$$

i.e., it is dominated by the osmotic pressure of counterions, which are accumulated inside the star volume. From eqs 11 and 14 we obtain the relation between the radial profiles of the polymer density and the degree of ionization.

$$\varphi(r) \approx f r^{-2}\sqrt{m/\alpha(r)} \tag{15}$$

For $\alpha \ll 1$, the combination of eqs 13 and 15 gives the radial profile of the degree of dissociation and of the polymer density:

$$\alpha(r) \approx \left(\frac{\alpha_b}{1-\alpha_b}\frac{m^{1/2}\Phi_b}{f}\right)^{2/3} r^{4/3} \quad (16)$$

$$\varphi(r) \approx f^{4/3} r^{-8/3}\left(\frac{1-\alpha_b}{\alpha_b}\frac{m}{\Phi_b}\right)^{1/3} \quad (17)$$

For the case of pH $\gg$ pK, $\alpha(r) \to 1$, eq 15 reduces to

$$\varphi(r) \approx \frac{f m^{1/2}}{r^2} \quad (18)$$

Subsequent integration of the density profile, $4\pi f \int_{R_{core}}^{R} \varphi(r) r^2 dr = fN$ provides an equation for the overall star size R as a function of structural parameters (f, N), salt concentration, and pH of the solution. The size R is given by

$$R \approx \begin{cases} [\alpha_b/(1-\alpha_b)] N^3 f^{-1} m^{-1} \Phi_b a & \text{for } \alpha_b/(1-\alpha_b) \sim 1 \\ N m^{-1/2} a & \text{for } \alpha_b \to 1 \end{cases} \quad (19)$$

where we have neglected the size of the core, R_{core}. The remarkable consequence of eq 19 is that the size *decreases* as a function of the number of arms and *increases* as a function of Φ_b for pH values around the pK. This is analogous to the behavior of the weak planar polyelectrolyte brush upon increasing the grafting density and/or the salt concentration in the osmotic regime.[23−26] The physical explanations of these effects are as follows: (i) Upon an increase in the number of arms, the number of charged monomers decreased because more and more counterions, i.e., protons, are retained within the star volume, thus reducing the degree of dissociation and the concomitant swelling. (ii) Upon an increase in the salt concentration, hydrogen ions inside the star corona are substituted by kationic salt ions. The decrease of the local proton concentration promotes ionization.

Salt Dominance Regime, $\alpha(r)\varphi(r)/m \ll \Phi_b$**.** This regime applies when the salt concentration in the bulk becomes larger than the concentration of mobile ions in the interior of the star. The asymptotics of eqs 10 and 12 for high salt concentrations are given by

$$\frac{\alpha(r)}{1-\alpha(r)}\frac{1-\alpha_b}{\alpha_b} \approx 1 - \frac{\alpha(r)\,\varphi(r)}{m\Phi_b} \quad (20)$$

$$\Delta\Pi(r)/k_B T \approx \alpha^2(r)\varphi^2(r)/2m^2\Phi_b \quad (21)$$

For high salt concentrations the degree of dissociation of the monomers in the star branches is the same as in the bulk. The polymer density distribution is found by using eqs 21 and 11:

$$\varphi(r) \approx f^{2/3} r^{-4/3}\left(\frac{m}{\alpha_b}\right)^{2/3} \Phi_b^{1/3} \quad (22)$$

The size of the star is therefore given by

$$R \approx N^{3/5} f^{1/5}\left(\frac{\alpha_b}{m}\right)^{2/5} \Phi_b^{-1/5} a \quad (23)$$

As follows from eqs 19 and 23, the size of a star at low pH passes through a maximum as a function of the ionic strength. The ionic strength Φ_b* at which this maximum occurs is found by equating eqs 19 and 23 and is given by

$$\Phi_b^* \approx m^{1/2}\alpha_b^{-1/2}(1-\alpha_b)^{5/6} f N^{-2} a^{-3} \quad (24)$$

2.3. Quasi-Neutral Regime. The quasi-neutral regime occurs when steric (nonelectrostatic) interactions between the arms dominate over the electrostatic ones, i.e., $\Delta\Pi_\theta(r)$ is the dominant term in eq 12. Close to the center of the star, this is for all regimes the case. On the scale of the star as a whole, the quasi-neutral regime occurs either at low pH (when ionization of arms is small) or at sufficiently large number of arms. (Upon an increase in the number of arms, the ionization of the arms is progressively suppressed, while the steric interactions get stronger.) In the quasi-neutral regime, the size of the star depends not on its charge but on the solvent quality. The size of the star scales therefore in the same way as for a neutral star. For a θ-solvent it is given by[20−22]

$$R \sim N^{1/2} f^{1/4} a \quad (25)$$

and the monomer density profile decays as

$$\varphi \sim r^{-1} \quad (26)$$

3. Numerical Self-Consistent-Field Model

The numerical SCF approach is based on the Scheutjens−Fleer (SF) algorithm. This algorithm was first proposed for neutral polymers at interfaces[18,27] and extended to account for electrostatics on a Poisson−Boltzmann level[28] and later generalized by van Male et al.[29] for spherical geometry and for calculating chemical reactions. All the calculations were done with the software package "sfbox" .[30] Some information on the SF−SCF model is given below; for full details the reader should consult the literature references quoted above.

The SF−SCF model is a self-consistent-field model; this means that, from a given distribution $\varphi_x(r)$ of all the particles in the system, a potential field $u_x(r)$ is calculated. From this field, which acts on the particles x, a new distribution is recalculated, and this is repeated until $u_x(r)$ and $\varphi_x(r)$ of all the particles is consistent. The subscript x is used to refer to the various types of particles. First we explain the way to calculate the field, $u_x(r)$, from the distribution, $\varphi_x(r)$, after which we proceed to calculate $\varphi_x(r)$ from $u_x(r)$.

The SF−SCF approach uses layers that are characterized by the (smeared out) volume fractions of the particles and by the total charge, i.e., a mean-field approximation. The thickness a of a layer is 0.6 nm. Every layer is totally filled. This means that in a liter $(10^{-3})/(N_{Av}(0.6 \times 10^{-9})^3) = 7.69$ mol "solvent" molecules are present. In the calculations the following particles x are used: solvent molecules (H_2O), salt ions (Na^+ and Cl^-), a nonionizable polymer segment (P_u), and a polymer segment with a pH-dependent charge (P_{pK}). The last type of segment can either be neutral or negatively charged depending on the pH. There are two types of salt ions in the system: co-ions Cl^- and counterions Na^+. The solvent molecule, water, can dissociate according to the following reaction: $2H_2O \leftrightarrows H_3O^+ + OH^-$ with a dissociation constant $K_w = 2.12 \times 10^{-16}$. A solvent molecule may take on three different *states* k, i.e., H_2O^0, H_3O^+, and OH^-. The value of the equilibrium constant K_w is the dimensionless equivalent of the

familiar water dissociation constant of 10^{-14} mol^2/L^2. The value of K_w depends on the thickness of the layer;[29] see also Appendix A.

The reaction of the polymer segment P_{pK} with water is

$$P^0_{pK} + H_2O \leftrightarrows P^-_{pK} + H_3O^+ \qquad K = 1.45 \times 10^{-6} \quad (27)$$

K is the dimensionless value of a pK_{acid} of 5 in the usual units. This means that at a local concentration of H_3O^+ of 10^{-5} mol/L half of the P_{pK} segments are dissociated. The polyelectrolyte stars are composed of three types of segments: P_u, P^-_{pK} (the charged form), and P^0_{pK} (the noncharged form).

The lattice layers are arranged in an array of concentric spherical shells numbered as $z = 1, 2, ..., M$; the outer surface of the zth layer is at the distance $r = R_{core} + z \times 0.6$, in nanometers, from the center, where R_{core} is the size of the core (see Figure 1). In the article we will use r for continuously changing sizes and distances, as for example are used in the analytical theory, and z for discrete steps in sizes or distances, e.g., in the numerical calculations. The dimensionless volume of layer z is $L(z)$ which is given by $^4/_3\pi(z^3 - (z-1)^3)$.

The SCF formalism features the particle potentials of state k, $u_{x,k}(z)$, which are conjugated to the volume fractions, $\varphi_{x,k}(z)$. The functions $u_{x,k}(z)$ and $\varphi_{x,k}(z)$ for a given particle type in state k are only functions of the z coordinate. Hence, all the local properties of the system are preaveraged over the angular coordinates (the spherical approximation). The total potential of a particle of type x in state k comprises three terms:

$$u_{x,k}(z) = u'(z) + k_BT\sum_{y,l}\chi_{x,k-y,l}(\langle\varphi_{y,l}(z)\rangle - \varphi_{b,y,l}) + \nu_{x,k}e\psi(z) \quad (28)$$

The first term is coupled to the incompressibility constraint $\sum_{x,k}\varphi_{x,k}(z) = 1$. The second term gives the short-range interactions, parametrized by Flory−Huggins interaction parameters $\chi_{x,k-y,l}$ between particle types x with state k and y in state l. This interaction of particle of type x with state k in layer z with a particle of type y in state l depends on the volume fraction of a particle of type y in state l positioned in layers $z-1$, z, and $z+1$. The site average volume fraction, denoted as $\langle\varphi_{y,l}(z)\rangle$, depends on $\varphi_{y,l}(z-1)$, $\varphi_{y,l}(z)$, and $\varphi_{y,l}(z+1)$ and is weighted by the geometry of the system.[31] The quantity $\varphi_{b,y,l}$ in eq 28 is the volume fraction of particles of type y in state l in the bulk. The third term accounts for the electrostatic contributions. The local charge density per layer $q(z)$ is given by $q(z) = e\sum_{x,k}\nu_{x,k}\varphi_{x,k}(z)$, where e is the elementary charge and $\nu_{x,k}$ the valence of the particle of type x in state k. The local electrostatic potential $\psi(z)$ is related to the local charge density $q(z)$ via the Poisson equation.

The way to find $u_{x,k}(z)$ from the volume fractions of all particles is given by eq 28. To calculate $\varphi(z)$ of a polymer from $u_{x,k}(z)$, one has to evaluate all possible and allowed conformations of the polymer in the potential field. The monomers in a polymer have a ranking number s which is ranging from 1 to N. In the case of a polymeric star one has to take into account the grafting constraint on the first segment. The chain statistics are treated in a first-order Markov approximation. Using this, we calculate the end-point distribution function $G(z,s|z^*,1)$ for the statistical weight of finding a chain fragment that starts with segment $s = 1$ at z^* (grafting point) and ends in layer z with segment s. Correspondingly, $G(z,s|N)$ is the statistical weight of all possible and allowed conformations, with the specification that segment $s = N$ can be anywhere in the system and segment s is again at coordinate z. Hence, $G(z,s|N)$ is the sum of $G(z,s|z',N)$ over all z'. The end-point distribution functions, in the approximation of first-order Markov chain statistics, obey the diffusion equation which, in discrete notation, can be written as

$$G(z,s|z^*,1) = G(z,s)\langle G(z,s-1|z^*,1)\rangle \quad (29a)$$

$$G(z,s|N) = G(z,s)\langle G(z,s+1|N)\rangle \quad (29b)$$

where $G(z,s)$ is the segmental weighting function and defined as $\sum_k\alpha_{b,k}G_k(z,s)$ with $\alpha_{b,k}$ the fraction of the segment at ranking number s in state k in the bulk and $G_k(z,s) = e^{u_{x,k}(z)/k_BT}$, where x is the particle type at ranking number s. $\langle G(z,s-1|z^*,1)\rangle$ and $\langle G(z,s+1|N)\rangle$ denote the site average end-point distribution of segment $s-1$ and $s+1$, respectively. The starting conditions for the propagators are $G(z,N|N) = G(z,N)$ for all z and $G(z^*,1|z^*,1) = G(z^*,1)$ (grafting condition). The density of a monomer with ranking number s follows from the composition law

$$\varphi(z,s) = C\,\frac{G(z,s|z^*,1)\,G(z,s|N)}{G(z,s)} \quad (30)$$

Here, the factor $G(z,s)$ in the denominator corrects for the double counting of the Boltzmann weight for segment s in the nominator. By summing eq 30 over s, we get the polymer density profile

$$\varphi(z) = \sum_{s=1}^{N}\varphi(z,s) \quad (31)$$

The normalization factor C is fixed by the number of monomers belonging to the star molecule:

$$C = \frac{f\,N}{\sum_{z=1}^{M}L(z)\,G(z,N|z^*,1)} \quad (32)$$

The grafting coordinate of the arms of the star z^* is chosen as close to the center as possible, i.e., $L(z^*-1) < f \le L(z^*)$. Hence for $f = 5$ we take $z^* = 2$, and for $f = 100$ we use $z^* = 4$.

The set of equations as presented in this section is closed but should be complemented by boundary conditions. As the cell is electroneutral as a whole, we set the "reflecting" boundary conditions at $z = M$, which guarantees that there are no gradients present in the z direction between $z = M$ and $z = M+1$; i.e., $\psi(M+1) = \psi(M)$, $u_{x,k}(M+1) = u_{x,k}(M)$, etc.

The above set of equations are solved iteratively by a Newton-like method. This results in the electrostatic potential profile and a distribution of number of charges per layer. Furthermore, the radial distributions of the salt ions, the polymer segments, and also, for instance, the end points of the branches are calculated.

The solvent is chosen to be a Θ-solvent for the polymer, i.e., $\chi = 0.5$ between the solvent molecules and the polymer monomers (see eq 28). Each polymer arm of the star has N monomers; every mth monomer can

dissociate. The average degree of dissociation per dissociating monomer $\bar{\alpha}$ is defined as

$$\bar{\alpha} = \frac{\sum_z \varphi_{P^-_{pK}}(z)\, L(z)}{\sum_z \varphi_{P_{pK}}(z)\, L(z)} \tag{33}$$

P^-_{pK} denotes the charged form of the dissociating polymer segment and P_{pK} the total number of dissociable monomers, i.e., $P_{pK} = P^0_{pK} + P^-_{pK}$. The volume fraction of the charged form of the P_{pK} monomer in a layer is coupled to the electrostatic potential in layer z through

$$\frac{\varphi_{P^-_{pK}}(z)}{\varphi_{P_{pK}}(z)} = \alpha(z) = \alpha_b e^{e\psi(z)/kT} \tag{34}$$

where $\psi(z)$ is the electrostatic potential in layer z.

As a measure for the size, the following definition of R is used:

$$R = \frac{\sum_{z=z^*}^{M} (z - z^*)\varphi(z,N)L(z)}{\sum_{z=z^*}^{M} \varphi(z,N)L(z)} \tag{35}$$

i.e., the first moment of the radial distribution of the end segments $\varphi(z,N)$, starting from the grafting point. The reason for using z^* as the starting point for the calculating the size is that we want to compare stars with different f. Therefore, we have to use a size that is comparable for all the stars. Because of the fact that stars with large number of arms have a small core, we have chosen to neglect the inner part and look upon the stretching from z^* on. The values of z^* are chosen to satisfy the volume requirements of a star.

To make a comparison with SANS experiments feasible, we need to calculate the scattering form factor from the radial distribution of the polymer segments. This is done through a Debye transformation. The form factor $P(q)$ for an object with a spherically symmetric density distribution is given by[16,32]

$$P(q) = \frac{1}{(Nf)^2} F(q)^2 \tag{36}$$

where Nf is the number of scattering units and $F(q)$ is form factor amplitude i.e., $F(q) = \int \varphi(z) e^{-iqz}\, dz$, the Fourier transform of the volume fraction profiles of the scattering units. Equation 36 is valid not only for star-shaped objects but also for polymeric micelles and small spherical particles with polymeric chains grafted to a surface. In the latter two cases, however, this validity applies only when the core is negligibly small or matched in scattering density with the solvent,[32] i.e., when the scattering is only due to the coronal chains. The scattering amplitude $F(q)$ (in discrete notation) is given by

$$F(q) = \sum_{z=1+Z_{core}}^{z=M+Z_{core}} \varphi(z) \int_{z-1}^{z} 4\pi z^2 \frac{\sin(qz)}{qz}\, dz \tag{37a}$$

$$= \frac{4\pi}{q^2} \sum_{z=1+Z_{core}}^{z=M+Z_{core}} \varphi(z)((z-1)\cos(q(z-1)) - z\cos(qz)) + \varphi(z)\left(\frac{\sin(qz)}{q} - \frac{\sin(q(z-1))}{q}\right) \tag{37b}$$

In this equation only the monomers of the polyelectrolyte scatter; z is the distance from the center, and Z_{core} is the number of layers that form the core to which the polyelectrolytes are grafted. In eq 37b the integration over one layer has been performed. The scattering wave vector q is limited by the number of layers used: $\pi/M \le q \le \pi$, because distances smaller than one layer or larger than M layers have no meaning. The factor π stems from 2π in the Fourier argument of the sine function, multiplied by the Nyquist critical frequency, $^1/_2$.[33] The step in q is π/M.

4. Results and Discussion

We will first show some overall features of the star molecule. Most calculations are done for $N = 200$, but in order to investigate finite size effects, some calculations were performed for $N = 1600$. The stars, calculated in this section, do not have a core, so if $z^* > 1$, then the inner part is penetrable for the polyelectrolyte. The number of the segments that will indeed go into the inner part is negligibly small. This means that the core is practically impenetrable. In section 4.1 the behavior at a low salt concentration is given. In the section 4.2 the effects, induced by changing the salt concentration, are investigated.

4.1. Annealed Polyelectrolyte Stars in a Solution with Low Ionic Strength. First the size and the average degree of ionization of a polyelectrolyte star on the pH will be shown. This will be followed by the evolution of the radial density profiles of the monomers and the radial profile of the degree of dissociation.

Changing the pH in experiments or in numerical calculations to obtain a desired dissociation automatically affects the ionic strength I. The ionic strength is defined as

$$I = A\frac{1}{2}\sum_i \nu_i^2 \varphi_{bi} = AI_b \tag{38}$$

Here, i denotes all small, mobile, ionic molecules, H_3O^+, Na^+, OH^-, and Cl^-, ν_i is the valence, φ_{bi} is the volume fraction of molecule i in the bulk, and A is a conversion factor needed to express the ionic strength in mol/L (see Appendix A).

Figure 2 shows the titration curves ($\bar{\alpha}$ vs pH) for the stars with different number of branches. (For comparison, the titration curve of an individual monomer in the bulk of the solution is plotted as well.) The shift of the titration curve to higher pH with increasing number of branches is clearly observed. There is a remarkable difference between a titration curve calculated with a constant ionic strength and one calculated with no added salt, for stars with different number of branches f. For the titration curves with constant ionic strength salt is added to keep the ionic strength constant while for the case when no salt is added, the pH is also a measure for the ionic strength. The titration of monomers in a polyelectrolyte star is influenced by their surroundings; for increasing number of branches the increase of the charge on the star is slower with

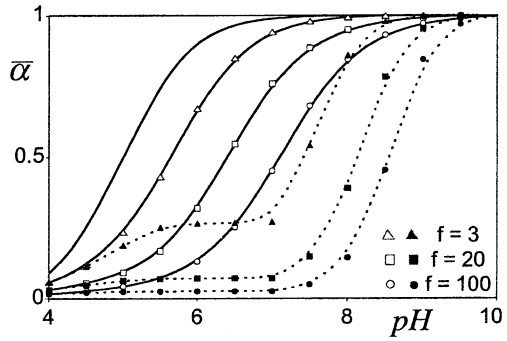

Figure 2. Average degree of dissociation as a function of the pH for different numbers of arms. Triangles denote $f = 3$, cubes $f = 20$, and circles $f = 100$. The closed symbols are the calculations without added salt and the open symbols the ionic strength is kept constant at 10^{-4} mol/L; the curve through the points are a guide to the eye. The curve without symbols denotes an individual monomer in the bulk.

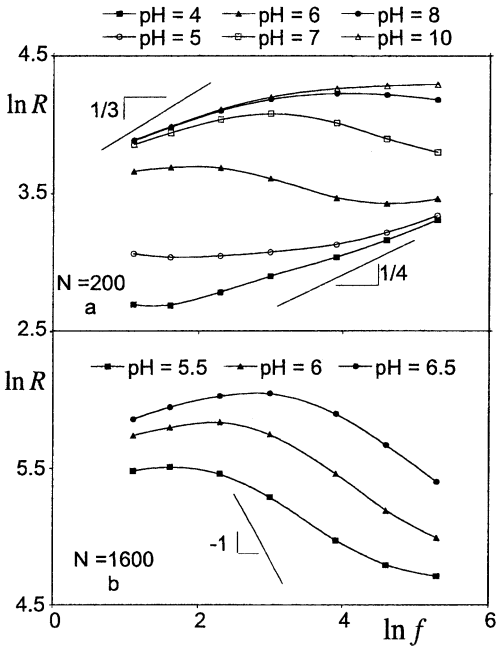

Figure 3. Size as a function of the number of arms f for $I = 10^{-4}$ mol/L, $m = 5$, pH as denoted in the graphs and $N = 200$ (a) or $N = 1600$ (b). Both graphs are in double-logarithmic scale. The curves are a guide to the eye. The straight lines show the predicted scaling behavior.

increasing pH (see Figure 2). For $f = 100$ and $I = 10^{-4}$ mol/L, at pH 7 half of the polymer segments are charged, $\bar{\alpha} = 0.5$, i.e., we see a shift of the apparent pK from 5 to 7. For the case of no added salt the shift is even larger. Furthermore, it can be seen from Figure 2 that for the system with no added salt the dissociation does not increase with increasing pH from pH = 4 to pH = 7. From pH = 4 to pH = 7 the ionic strength decreases by a factor of 1000, and the low ionic strength prevents dissociation. Upon further increasing the pH, the ionic strength increases again and the dissociation becomes possible. This rather special behavior can only be measured if one starts with a salt-free solution at pH = 7 and then goes to either pH = 4 or pH = 10.

Further on in this section the ionic strength I is kept constant and low. For the highest acid or base concentration, i.e., pH = 4 or pH = 10, the ionic strength is 10^{-4} mol/L, even if no extra salt is added. To keep the ionic strength in the bulk constant and equal to 10^{-4} mol/L while varying pH, extra salt is added in the range of pH's between 4 and 10.

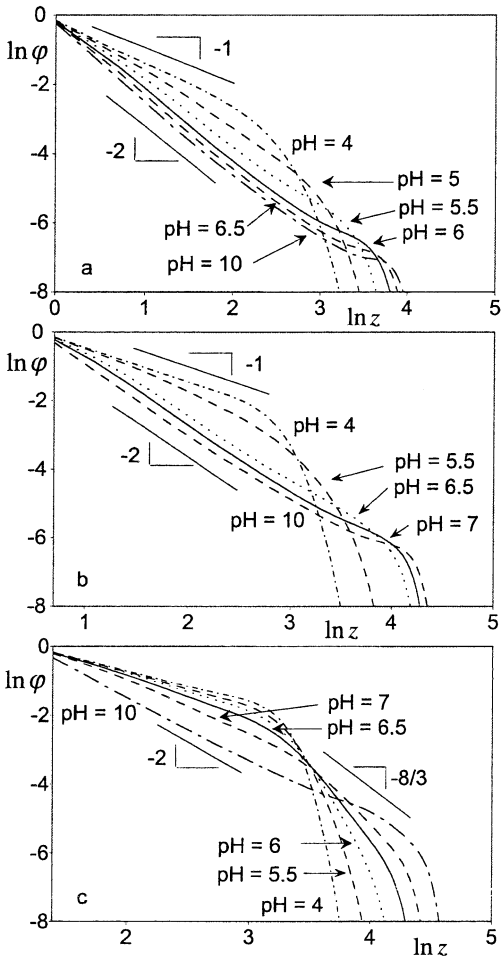

Figure 4. Double-logarithmic plot of the volume fraction of the polyelectrolyte as a function of the distance from the center z for $I = 10^{-4}$ mol/L, $m = 5$, pH as denoted in the graphs and $N = 200$ for $f = 3$ (a), $f = 20$ (b), and $f = 100$ (c).

In Figure 3 the size of a star is shown as a function of the number of arms f, for different values of pH, with $m = 5$ and $N = 200$ (Figure 3a) or 1600 (Figure 3b). It can be seen that for constant f the size increases with the pH; this is due to an increasing ionization of the branches. At low pH, i.e., small $\bar{\alpha}$, in Figure 3a the size increases monotonically with the number of arms due to an enhanchment of the steric interactions. At pH = 4 the slope of ln R vs ln f is close to $^1/_4$, which is predicted for a neutral star in Θ-solvent (see eq 25). For high pH (i.e., pH ≥ 8) the star size grows for increasing f at small f and flattens off at larger f, just as for quenched polyelectrolyte stars.[6–8] The small increase with f means that the star is in the polyelectrolyte regime (see eq 3). The most interesting behavior is found for intermediate pH, i.e., pH ≳ pK. The size exhibits a maximum as a function of f for 5.5 ≤ pH < 8. The weak increase, because the star is still in the polyelectrolyte regime, is followed by a sharp decrease in size with increasing number of branches. This maximum is seen for pH 6 and 7. As discussed in section 2.2, the decrease in the star size as a function of the number of branches is due to suppressed ionization. In the osmotic annealing regime a power law exponent of −1 is expected (see eq 19); the slopes found in Figure 3 are smaller. This is due to increasing steric repulsion between the branches,

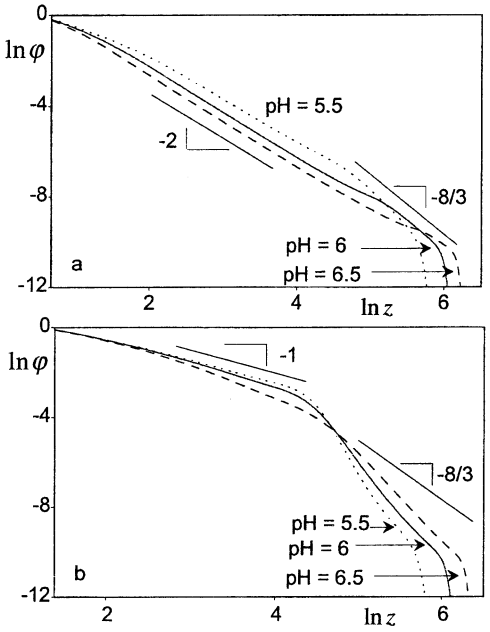

Figure 5. Double-logarithmic plot of the volume fraction of the polyelectrolyte as a function of the distance from the center z for $I = 10^{-5.5}$ mol/L, $m = 5$, $N = 1600$, and pH as denoted in the graphs. (a) $f = 20$ and (b) $f = 100$.

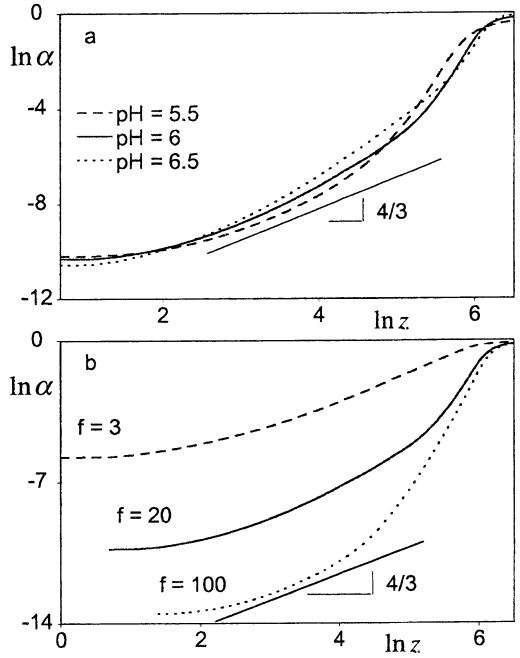

Figure 6. Degree of dissociation as a function of the distance from the center z for $I = 10^{-5.5}$ mol/L, $m = 5$, and $N = 1600$. (a) $f = 20$, pH as denoted in the graph. (b) The pH is 6 and f as denoted in the graph; both plots are in double-logarithmic scale.

which is not taken into account in eq 19. This decrease in size is more clearly seen in Figure 3b, due to the less pronounced steric interactions for the star with longer branches. By comparing the stars with $N = 200$ and $N = 1600$, it can be concluded that the finite size effects are small and the main features, which are analytically predicted, are already seen for $N = 200$.

In Figure 4 the segment density is plotted vs the distance from the center in double-logarithmic coordinates, for a range of pH values, three different values of f, and $N = 200$. The volume fraction of the polymer segments decreases with distance from the center. The decrease becomes steeper with increasing pH, due to the increasing number of charges on the chain. With increasing number of arms the susceptibility for changes to the pH decreases; compare the degree of dissociation for $f = 3$ and $f = 100$ in Figure 2, and furthermore the difference in R between pH 4 and 6 for f is 3 and 100 in Figure 3a. This is due to increasing importance of steric interactions. For low pH the slope of the ln φ vs ln z curve is close to -1, which is expected for uncharged stars (see eq 26).[7] For high pH, the situation is similar to that of quenched stars; the observed slope is close to -2, as expected for the case of uniformly extended branches according to eq 18. For intermediate pH a decrease faster than z^{-2} is seen for $f = 100$ at the periphery of the star. The extra extension is due to a gradient in the ionization of the branches. The predicted decrease of $-8/3$ (see eq 17) is not confirmed, however. This may be due to the limited size of the arms; therefore, we turn to the results for $N = 1600$.

In Figure 5 the volume fraction profiles of a star with 20 and 100 branches is shown; each branch has 1600 monomers. In Figure 5a, where $f = 20$, a steep slope is observed at the periphery of the star. In Figure 5b for $f = 100$, the steep decrease of the volume fraction profiles with z is even better seen. In the region of this steep slope of ln φ vs ln z, the local tension of the arms is an increasing function of z due to increasing ionization. The effect of increasing number of branches can be clearly seen: for $f = 20$ at the periphery, a small region $\varphi(z) \sim z^p$, with $p < -2$ can be observed, and for $f = 100$ this region occurs over a larger z range. The power law exponent for $f = 100$ is even more negative than the predicted $-8/3$ (see eq 17).

The volume fraction decay of z^{-2} for $f = 20$ in Figure 5a is larger than expected, which is based on the charge of the star (see Figure 6a). A z^{-2} decay of the volume fraction is expected for a fully charged star. The expected decay for a noncharged star is $\varphi(z) \sim z^{-1}$. This fast decay is probably due to the pulling of the ends of the star branches, which like to stretch due to their charge.

The decay of the volume fraction profiles faster than z^{-2} indicates an increase in the ionization of the arms; this is shown in Figure 6. This figure shows clearly the large increase in ionization of the branches with distance from the center. The fraction of charged monomers increases toward the periphery of the star, $\alpha \rightarrow \alpha_b$. However, the expected power law dependence for $\alpha(r) \sim r^{4/3}$ (see eq 16) is observed at smaller z values than the fast decay of the volume fraction profiles plotted in Figure 5. The faster than predicted $z^{4/3}$ increase of the ionization at the periphery of the star is in agreement with the faster than predicted $z^{-8/3}$ decrease of the volume fraction profiles in Figure 5b. In Figure 6b, the radial increase of the degree of dissociation from the center to the periphery for $f = 100$ is most pronounced, the dissociation is negligible in the inner region of the star, where the power law dependence of $\varphi(z) \sim r^{-1}$ occurs, and it increases to α_b at the end of the arms.

The profiles of the degree of dissociation are represented in Figure 7 and clearly demonstrate a linear dependence of $\log(1 - \alpha)$ vs z^2 in the periphery of the star. This linear dependence was predicted by analytical SCF theory for annealed planar brushes.[24] Hence, we find the structure of the annealed star at the outer edge does not depend on the curved geometry anymore and resembles that of a planar polyelectrolyte brush.

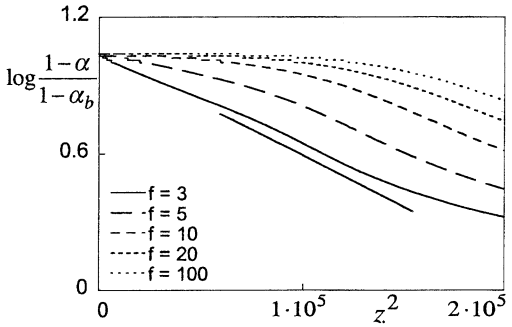

Figure 7. log [(1 − α)/(1 − α_b)] as a function of z^2 for $I = 10^{-5.5}$ mol/L, $m = 5$, and $N = 1600$, and pH 6 for different number of arms.

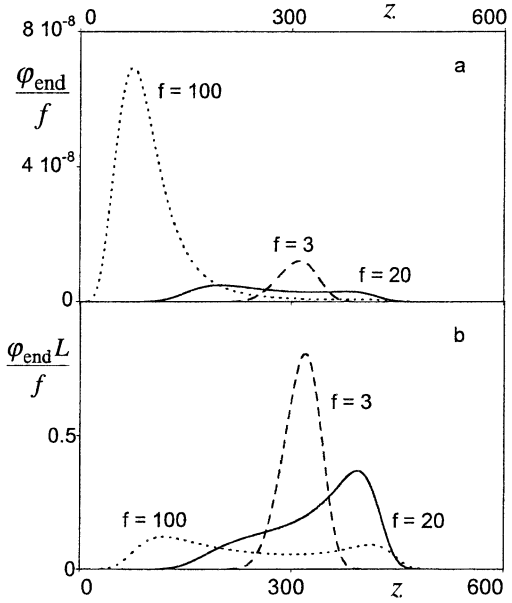

Figure 8. Volume fraction and the total number of the end segments as a function of z in (a) and (b), respectively. Both the volume fraction profiles and the profiles of the total amount of end segments are normalized by f. The other parameters are $m = 5$, pH = 6, $N = 1600$, $I = 10^{-5.5}$ mol/L, and f as denoted in the graphs.

The distribution of end points is an interesting property which is easily obtained in the SCF calculations but not from analytical theory. In Figure 8 the volume fraction (a) and total number (b) of the end segments of the polyelectrolyte star per layer are shown. To facilitate a comparison between stars with different number of arms, the volume fraction and the total number are normalized with respect to the number of arms. (The total number of segments gives extra information especially because the lattice is spherical and the size R, defined in eq 35, is determined by the number of segments in a layer and not by the volume fraction.)

For stars with a small number of branches (the polyelectrolyte regime), e.g., $f = 3$, in Figure 8a we observe a "Gaussian" shape of the free end distribution function. It peaks close to the periphery of the corona, and we find a wide zone, where no free ends occur, in the central region of the star (a dead zone). For $f = 20$ the free ends distribution is much broader and skewed (see Figure 8a). One maximum of the curve is shifted to lower z value, as compared to the ends distribution for the star with $f = 3$ branches. This shift of the maximum is related to the suppressed ionization upon

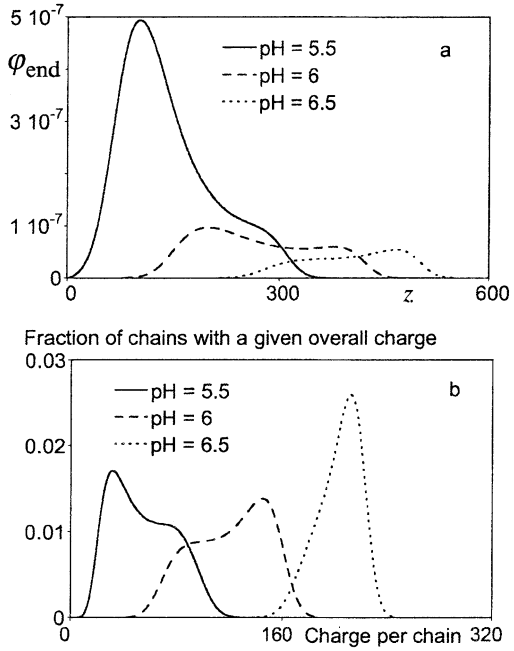

Figure 9. End-point radial distribution profiles for different pH are shown in (a). In (b), the fraction of chains with a specific number of charges on the arm as a function of the number of dissociated groups on one arm is given. Other parameters of the star are $N = 1600$, $f = 20$, $m = 5$, and $I = 10^{-5.5}$ mol/L.

an increase in the number of branches. The maximum at higher z value is due to some star arms which are more charged and therefore more stretched. For $f = 100$ the distribution exhibits a maximum and a long tail. The position of the maximum is shifted to even smaller z, as compared to the distribution of the ends in a star with $f = 20$ branches. Because of the high local polymer density, the chains having ends close to the maximum of the distribution are weakly charged, while more strongly charged (and therefore stronger extended) chains contribute to the tail of the distribution.

Figure 8b, where the total amount of the end points per layer is given for $N = 1600$, shows for $f = 100$ two maxima and for $f = 20$ a very broad distribution with a shoulder. (For $N = 200$ the end-point distribution is unimodal but exhibits a weak shoulder (not shown).) One can think that these two maxima indicate two populations of chains which stem a choice a chain can make: it can either dissociate weakly and remain weakly extended, or it can dissociate substantially, resulting in strong electric repulsion and significant stretching. Figure 9a demonstrates the evolution of the end profiles as a function of the pH. With an increase in the pH, the two populations remain, but the maxima of the distribution are shifted to higher z value. Figure 9b shows the probability distribution of the number of charges on an arm. On the x-axis the number of dissociated segments on an arm is plotted, irrespective of the position of these dissociated segments on the arm. The way to calculate the probability of finding a branch with a certain amount of charges is described in Appendix B. Figure 9b shows that there are two populations of arms with respect to their charge for pH 5.5 and 6 but not for pH ≥ 6.5 even though at this pH the end-point distribution is also bimodal.

Even though we see two populations of end points and at some pH's also two populations of charged chains, we do not expect a "phase" transition between branches

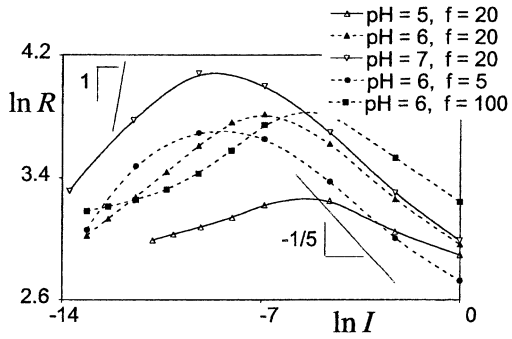

Figure 10. Size of an annealed star as a function of the ionic strength, for $N = 200$, $m = 5$, pH and number of arms f as denoted in the graph.

which are hardly charged and ones which are more ionized. Because for some calculations where a bimodal distribution in end points was seen, do not show a bimodal distribution in the fraction of charges per chain, and a second reason is that the amount of charges varies gradually when changing the pH. Other reasons not to expect a phase transition due to the amount of charges on a branch is because the two maxima in the distribution of end points have also been predicted by analytical SCF models for planar quenched brushes.[34,35]

4.2. Behavior of Annealed Polyelectrolyte Stars upon Changing the Ionic Strength. Increasing the salt concentration has two competing effects on the radius R of the star. The most common effect is the screening of the charges: with an increase in the salt concentration the electrostatic repulsion between the arms gets weaker. Therefore, the size of the star decreases with increasing salt concentration namely (according to eq 23) as $R \sim \Phi_b^{-1/5}$, provided the salt concentration outside the star volume is larger than the concentration of counterions inside the star volume. The other effect is due to the fact that H^+ and OH^- do not only contribute to the ionic strength but also participate in the dissociation equilibrium, thereby determining the charge of the polyelectrolyte. At not too high pH, addition of salt in the bulk of the solution results in progressive substitution of H^+ ions inside the star volume by Na^+ ions and, hence, in an additional ionization followed by an extension of the star arms. As long as the (simultaneously increasing) screening of the Coulomb interactions can be neglected, the scaling theory predicts a linear *increase* of the star size with increasing salt concentration: $R \sim \Phi_b$ according to eq 19. The latter effect is only seen for low ionic strength. Altogether, the increase in the ionic strength will at first lead to an increase in the size, and when the ionic strength in the bulk solution becomes larger than that inside the star volume, it causes a decrease in size; i.e., a maximum of the size as a function of salt concentration is expected.

The size of the stars as a function of the ionic strength is shown in Figure 10; a clear maximum is indeed observed in all cases. We observe, after the maximum, a slope slightly smaller than $-1/5$, due to the increasing importance of steric repulsion at large I. However, the power law dependence of R on Φ_b in the annealed osmotic regime (low salt) is much weaker than $R \sim \Phi_b$, due to the fact that an increase in the salt concentration results simultaneously in stronger screening of the repulsion between ionized monomers. The maximum in size for an annealed star or curved brush is also found experimentally for some systems.[36,37]

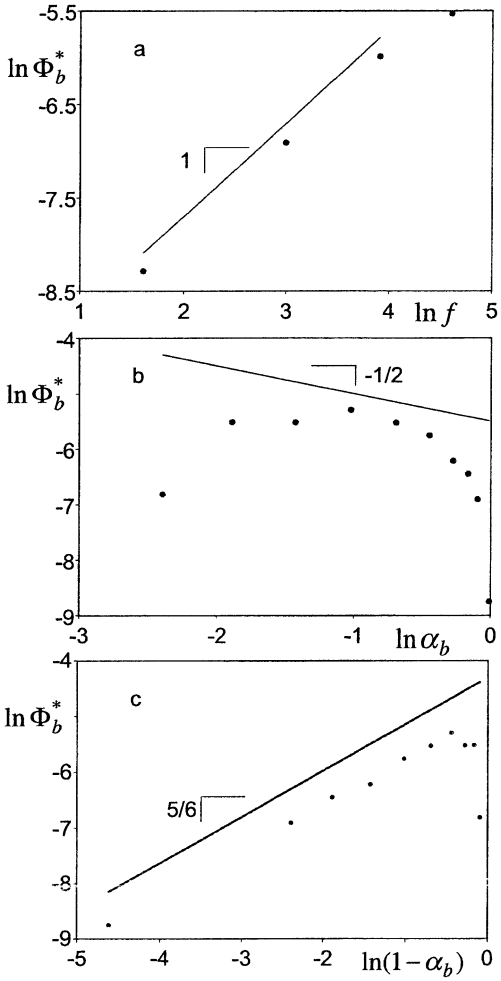

Figure 11. Dependence of the salt concentration Φ_b^* at which the star size is maximal on the number of arms (a) and the degree of dissociation (b, c). The parameters are $N = 200$, $m = 5$, in (a) the pH is 6, and in (b) and (c) $f = 20$.

The salt concentration Φ_b^* at which the maximum in the star size is observed depends on f and α_b (see eq 24). In Figure 11 we see a linear increase of Φ_b^* with the number of arms (Figure 11a) and a maximum in Φ_b^* with increasing bulk degree of dissociation α_b (Figure 11b,c). The proportionality between Φ_b^* and f, predicted by eq 24, is nicely confirmed.

In Figure 11b the dependence of Φ_b^* on α_b is shown. The exponent of the power law dependence, predicted as $\alpha_b^{-1/2}$ (see eq 24), is not observed. To explain this, we have to make a distinction between the low degree of ionization and the high degree of ionization in the bulk. For the small α_b, the electrostatic interactions not only determine the star conformation but also steric interactions. Furthermore, the star size does not change dramaticly with increasing ionic strength.

The reason why for large α_b the theoretical dependence of Φ_b^* on α_b is not observed may be related to the underestimation of the screening of the electrostatic repulsion for $\Phi_s < \Phi_s^*$. This was also noted when we discussed Figure 10. The dependence of R on the ionic strength is much weaker than the predicted linear dependence.

The dependence of Φ_b^* on $1 - \alpha_b$ is shown in Figure 11c. The exponent of the power law dependence, $5/6$, is found.

The last part of this section is addressed to the volume fraction profiles. For a star with 20 arms, $m = 5$ or 1,

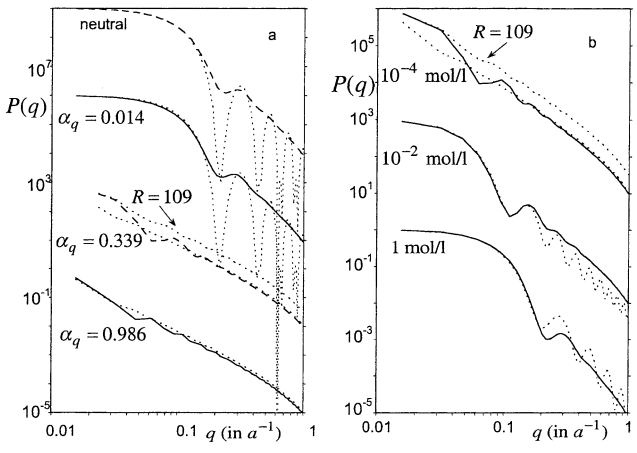

Figure 12. Form factor $P(q)$ for a quenched star with $N = 200$, $m = 1$, and $f = 20$ in a Θ-solution. The dotted lines show the form factor calculated for volume fraction profiles with a single-power-law decay. In (a) the ionic strength is 10^{-4} mol/L for a star with different number of charge per monomer α_q (as indicated in the graph); in (b) a quenched star with $\alpha_q = 0.339$ per monomer at different ionic strengths (concentrations are shown in the graph) is shown. The different calculations are shifted by multiplication factor of 1000. The parameters for the one-power-law decay are denoted in Table 1.

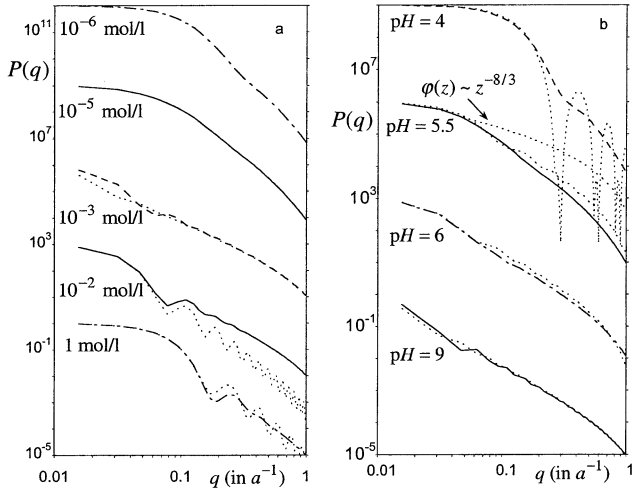

Figure 13. Form factor $P(q)$ for an annealed star with $N = 200$, $m = 1$, and $f = 20$ in a Θ-solution. The dotted lines show the form factor calculated for volume fraction profiles with one-power-law decay. In (a) the pH = 6 and the ionic strength is varied, in (b) the ionic strength is constant, $I = 10^{-4}$ mol/L, and the pH is changed. The different calculations are shifted by multiplication factor of 1000. The parameters for the one-power-law decay are denoted in Table 1.

at pH 5 or 6, and $N = 200$, the volume fraction profile decays at low ionic strength as z^{-1}, as for neutral stars. An increase in the ionic strength induces ionization and the polymer density profile decays as z^{-2}, a further increase in the ionic strength leeds to screening of the charges on the arms. In this last regime the volume fraction profiles show a $\varphi(z) \sim z^{-4/3}$ decay (see eq 22). Any new information is not gained from these volume fraction profiles, and therefore they are not shown.

4.3. Form Factors of Star-Shaped Polyelectrolytes. A good technique to measure the internal structure and the size of a small object is SANS. The measurements give the scattering intensity as a function of the wave vector q. From the intensity the form factor $P(q)$ can be obtained at sufficiently low concentration. The form factor $P(q)$ is directly related to the shape of the concentration profile by eq 36. So we explicitly calculate form factors from our volume fraction profiles. For comparison, we also calculate $P(q)$ for a single-power-law density profile, $\varphi(z) \sim z^p$. In Figures 12 and 13, we present the form factors of a quenched and of an annealed polyelectrolyte star, respectively.

In Figure 12a we see that upon increasing the charge on the branches the initial decay of $P(q)$ gets faster, which indicates an increasing size of the star, as expected for quenched stars.[8] Simultaneously, the first minimum in $P(q)$ shifts to smaller q value. The low q region for the noncharged star is nicely described by the form factor obtained with a volume fraction profile, decaying as z^{-1}, although volume fraction profiles with $\varphi(z) \sim z^p$ in which $p < -1$ fit the calculated form factor even better. The $P(q)$ for the star with $\alpha_q = 0.986$ is mimicked fairly well by a form factor resulting from $\varphi(z) \sim z^{-2}$. The $P(q)$ for the star with $\alpha_q = 0.339$ cannot be fitted using a single-power-law decay of the density profile; the low q region can be fitted with a $P(q)$ obtained with a profile of $\varphi(z) \sim z^{-2}$, and $R =$ log, but $P(q)$ at the high q range has the same shape as that of that of the star with a charge of $\alpha_q = 0.986$.

Figure 12b shows the effect of varing the ionic strength. With decreasing ionic strength the star size grows. The star passes from the salt dominance regime, $\varphi(z) \sim z^{-4/3}$, to the osmotic regime, $\varphi(z) \sim z^{-2}$. The $P(q)$ curves for the lowest salt concentrations (10^{-4}, 10^{-5}, and 10^{-6} mol/L) have an identical shape (therefore, the latter two are not shown).

The effect of different ionic strengths for an annealed polyelectrolyte is shown in Figure 13a. The high salt concentrations give the same trends for annealed and quenched stars, i.e., the same exponent $p = -4/3$ for the power law polymer density decay and a decreasing size with increasing the salt concentration. The salt ions only screen the charge but do not affect the degree of dissociation. In contrast, for the low salt concentrations, i.e., 10^{-5} and 10^{-6} mol/L, the shape of the form facters is totally different from those of the quenched star. The $P(q)$ for these salt concentrations is smooth and cannot be fitted with a single-power-law density decay. By changing the salt concentration from 10^{-3} to 10^{-6} mol/L, the initial decay of $P(q)$ becomes smaller, and the oscillations disappear. The former indicates a decrease in size of star due to suppressed ionization. This is expected because in Figure 10 the star with $f = 20$ and at pH 6 has its maximum in size at $\ln I = -7$, i.e., at $\approx I = 10^{-3}$ mol/L.

By comparing Figures 12b and 13a, the qualitative difference in the behavior of the form factors of an annealed and a quenched star with changing the salt concentration is clearly seen. The $P(q)$ of the annealed star loses most of its structure with decreasing the salt concentration while that for the quenched star exhibits pronounced oscillations in the whole range of salt concentrations.

In Figure 13b the effect of increasing the pH, i.e., the amount of charges on the branches, at a constant ionic strength is shown. The form factors decrease faster as a function of q with increasing pH, which is an indication for an increasing size of the star. In Figure 13b we see at pH 4 and 9 the form factor has pronounced oscillations in contrast to pH 5.5 and 6. The $P(q)$ curve at pH 4 resembles that for a neutral star and can be fitted with a density profile of $\varphi(z) \sim z^{-1}$. The $P(q)$ at pH 9 can be fitted by the $\varphi(z) \sim z^{-2}$ decay just as for a fully charged star (compare Figure 13a). At intermediate

Table 1. Parameters Used for Fitting of the Form Factors of Quenched and Annealed Stars, with a Single-Power-Law Decay[a]

system	I (mol/L)	$\varphi(z) \sim z^p$	R_{star}	R_{core}
neutral		$p = -1$	28	1
quenched, $\alpha_q = 0.014$	10^{-4}	$p = -1$	28	1
quenched, $\alpha_q = 0.339$	10^{-4}	$p = -2$	109	1
		$p = -2$	180	1
quenched, $\alpha_q = 0.986$	10^{-4}	$p = -2$	180	1
quenched, $\alpha_q = 0.339$	10^{-4}	$p = -2$	109	1
		$p = -2$	180	1
quenched, $\alpha_q = 0.339$	10^{-2}	$p = -4/3$	58	0
quenched, $\alpha_q = 0.339$	1	$p = -4/3$	31	1
annealed, pH = 6	10^{-6}	*b*		
annealed, pH = 6	10^{-5}	*b*		
annealed, pH = 6	10^{-3}	$p = -2$	180	1
annealed, pH = 6	10^{-2}	$p = -4/3$	81	0
annealed, pH = 6	1	$p = -4/3$	36	1
annealed, pH = 4	10^{-4}	$p = -1$	21	1
annealed, pH = 5.5	10^{-4}	$p = -8/3$	100	1.5
		$p = -2$	60	1.5
annealed, pH = 6	10^{-4}	$p = -2$	100	1.5
annealed, pH = 9	10^{-4}	$p = -2$	195	1

[a] The core size for a star is $(z^* - 1)$ layers large, where z^* is the layer where the arms are grafted. For a star with 20 arms, the grafting layer is 2 and therefore the core is 1 layer thick. [b] Cannot be fitted with one exponent.

Table 2. Parameters[a] Used for the Calculation of the Polymeric Micelles That Can Be Compared with the Experimental Results of Groenewegen et al.[16]

parameter	value
no. of monomers, N	120
no. of arms, f	100
m	1
solvent quality	θ
ionic strength	10^{-4} mol/L
pK	5
dielectric constant of the core	$2\epsilon_0$
radius of the core R_{core}	6×0.6 nm
radius of the cell D	206×0.6 nm

[a] The polystyrene core is known to be hydrophobic. In the numerical calculations it is possible to take this into account but it hardly effects the volume fraction profiles and even less the form factors. Therefore, the results of these calculations are not shown.

Table 3. Parameters for the Single-Power-Law Decay of the Volume Fraction Profiles Used To Fit the Calculated Form Factors in Figure 15

pH	$\varphi(z) \sim z^p$	R_{star}	R_{core}	
4	$p = -1$	18	6	dashed line
5	$p = -1$	18	6	dashed line
5	$p = -1$	19	6	dashed line
5	$p = -8/3$	35	10	dotted line
6.5	$p = -8/3$	50	8	dotted line
6.5	$p = -2$	40	6	dashed line
6.5	$p = -2$	40	6.5	dashed line
8	$p = -2$	95	6	dashed line
9	$p = -2$	100	6	dashed line

pH values, where the number of charges on the star branches is gradually increasing, the form factors cannot be fitted by those calculated with one power law density decay. From the analytical theory one expects for these intermediate values of pH the combination of a $\varphi(z) \sim z^{-1}$ and a $\varphi(z) \sim z^{-8/3}$ density profile (in the central and in the peripherical region of the star corona, respectively). Therefore, the form factor calculated with the volume fraction profile with a single-power-law volume fraction profile of $\varphi(z) \sim z^{-8/3}$ does not provide a good fit for the $P(q)$ curves.

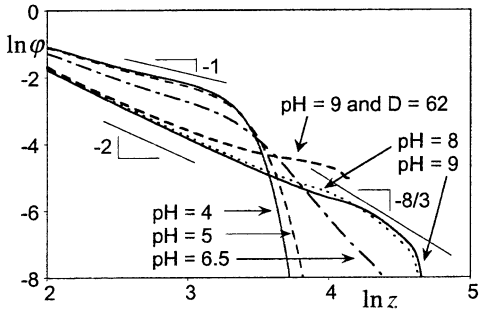

Figure 14. Volume fraction of the polyelectrolyte micelle as a function of the distance from the center z in double-logarithmic scale. The pH is denoted in the graphs. The parameters of the polyelectrolyte micelle are denoted in Table 2.

At the high q region, the $P(q)$ is very sensitive to the size of the core, especially for the profiles with a strong decay, i.e., $\varphi(z) \sim z^{-2}$ or $z^{-8/3}$.

5. Comparison with Experiment

The calculated $P(q)$ curves (Figures 12 and 13) give the general trends for the expected behavior of the form factors for star-shaped polyelectrolytes. Now we want to compare our calculations directly to a recent SANS experiment with polymeric micelles with annealed polyelectrolytes as the coronal chains. Groenewegen et al.[16] used a diblock copolymer of polystyrene/poly(acrylic acid) (PS/PAA), which associate in aqueous solutions to form micelles. The core is formed by the PS block and has an average size of 4.5 nm. The number of polymers associated in one micelle was about 100. This number was calculated from the core size, using the density of poly styrene and by normalizing the partial form factor of PS−PS. Groenewegen et al.[16] have fitted the measured form factors with those obtained from volume fraction profiles with a one power law decay and found that $\varphi(z) \sim z^p$ with $p < -2$ provides the best fit for their experimental data at low degree of ionization.

To compare the measured data, we use the parameters listed in Table 2. For the polymeric micelles studied by Groenewegen et al.,[16] it was shown that the variation of pH and/or salt concentration does not affect the aggregation number and therefore also not the core size. Therefore, these micelles can be modeled like star polymers with fixed number of arms grafted to an impermeable core of a given size. The parameters used are partially given by Groenewegen et al.[16,17]

Figure 14 shows the volume fraction profiles calculated for the above-mentioned system. It is seen that for pH 4 and 5 the volume fraction of the polymer segments decreases as z^{-1} and for pH 8 and 9 as z^{-2}. Analytical theory predicts these decays for noncharged and fully charged stars, respectively. At pH 6.5 a transition between the fully charged and the noncharged state is seen. The volume fraction profile shows a wide range with a radial density decay, which is faster than z^{-2}.

The volume fraction profile for a smaller cell size is just shown for comparison. The size of the cell is related to the micellar concentration; $D = 62$ is obtained from the given concentration of 0.093 mol PAA/L, the degree of polymerization (120), and the aggregation number of the micelle (100). The average distance between two polyelectrolyte micelles can be calculated from the concentration of hydrophobic PAA x, the aggregation number f, and the degree of polymerization N. Every

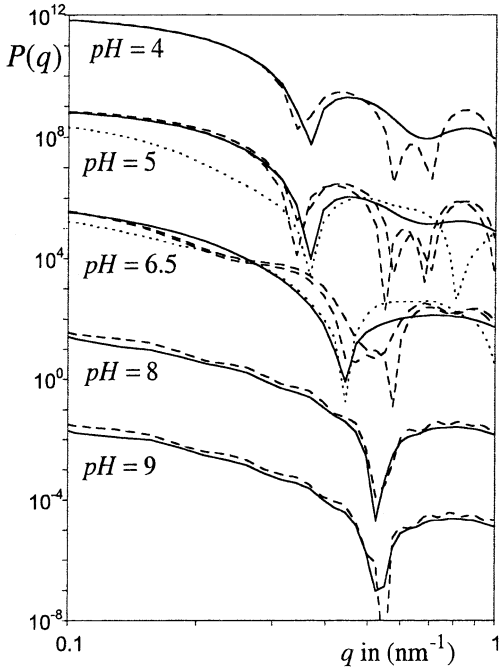

Figure 15. Calculated form factors of a polyelectrolyte micelle, $I = 10^{-4}$ mol/L, $D = 200$, and the pH as denoted in the graph. The dashed and dotted lines are the calculated form factors for a single-power-law decay; the parameters are listed in Table 3. The form factors for the different pH's are shifted along the *y*-axis by multiplication factor of 1000.

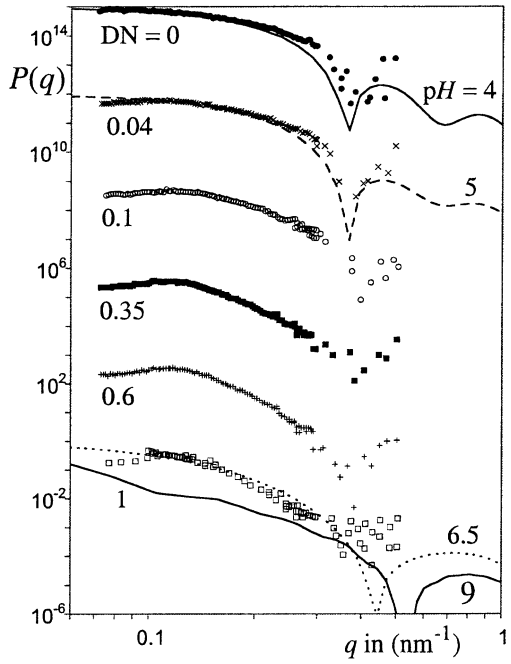

Figure 16. Data of Groenewegen et al.[16] (symbols) for different degree of neutralization (DN) compared with the calculated form factors of a polyelectrolyte micelle, $I = 10^{-4}$ mol/L, $D = 200$ (lines). The degree of neutralization is the ratio of added moles of base per monomers of acrylic acid present in the solution. The form factors for the different degrees of neutralization are shifted along the *y*-axis by a multiplication factor of 1000.

polymer has a volume of N/xN_{Av} liter available, in which N_{Av} is Avogadro's number. The volume occupied by one micelle is then Nf/xN_{Av}; from this volume one can easily calculated the average distance between two micelles and the dimensionless radius of the cell D.

Only at high pH, where the micelle is fully charged there is a difference between $D = 62$ and $D = 206$. Further on we will use the data collected for a cell with 206 layers.

To be able to compare directly with the measured data of Groenewegen et al.,[16] we calculate the scattering form factor from the volume fraction profiles using eq 36.

In Figure 15 the calculated form factors are shown. With increasing pH the $P(q)$ curves decrease faster, which indicates a larger size for the micelles. The first minimum in $P(q)$ for pH 4 and pH 5 is at $q = 0.37$ nm^{-1}, which is in good agreement with the experiment (see also Figure 16). This minimum shifts to larger q with increasing pH. This shift of the minimum to higher q indicates a change in the shape of the density profile.

We have fitted our calculated form factors with form factors for a single-power-law decay. For pH 4, 5, 8, and 9 this leads to good fits. As was already mentioned for these pH's, the volume fraction profiles show just one regime with a clear power law behavior ($\varphi(z) \sim z^{-1}$ for pH 4 and 5 and $\varphi(z) \sim z^{-2}$ for pH 8 and 9). At pH 6.5 a good fit to the calculated form factors is hardly found; a volume fraction with a density decay as $\varphi(z) \sim z^{-2}$ gives a form factor with a minimum at too high q. The density decay of $z^{-8/3}$ gives a the minimum at the right q value but only if the size of the core is set larger than it was. Furthermore, at low q this form factor of the single-power-law decay gives a lower value for $P(q)$.

In Figure 16 the numerical form factor is directly compared with the data given in Figure 6 of Groenewegen et al.[16] The degree of neutralization is an easy experimental accessible parameter, which gives an indication of the change in the degree of dissociation α. The actual degree of dissociation depends for the same degree of neutralization on the concentration of the polyelectrolyte; we therefore used the pH which is directly related to the degree of dissociation, via eq 1.

From Figure 16 it can be seen that the data of the DN of 0, 0.04, and 1 can be reasonably well be described by the calculated form factors of respectively pH 4, 5, and 6.5. The form factors of the degree of neutralization between 0.04 and 1 change gradually, the minimum shifts to larger q, and the slope of $P(q)$ gets steeper. These features are obtained also from the calculated form factors. The surprising part is that the high degree of neutralizations are not well described by the form factors of pH 9 but by the form factor of pH 6.5. Furthermore, we conclude from the experimental and the numerical results that with increasing pH: (i) Both calculated and measured formfactors exhibit faster initial decay. (ii) The first minimum in $P(q)$ is shifted in the calculated curves to larger q while in the measured curves the minimum gets broader and also shifts to larger q.

6. Conclusion

We have investigated the conformational structure of annealed polyelectrolyte stars in dilute solutions as a function of the number of arms, the ionic strength, and the pH of the solution. This has be done by means of detailed numerical SCF calculations, which complement the analytical scaling theory.[7] The calculations confirm the specific behavior of annealed stars vs quenched stars and enable us also to (i) study the intrinsic structure of an annealed star, (ii) calculate measurable properties of an annealed star, and (iii) indicate the parameter range where the specific effects of annealed stars are expected in experiments.

A maximum in the size with increasing number of arms or with increasing salt concentration is found. The salt concentration at which this maximum occurs is directly related to the internal charge density.

For pH ≈ pK we have found that the radial decay of the polymer density occurs faster than in a quenched polyelectrolyte star, i.e., $\varphi(z) \sim z^p$, with $p < -2$, which was predicted by analytical theory. There remains only a small question; in some calculations this fast decay of the volume fraction profile at the end of the star is preceded by a decay of z^{-2}. This decay is expected for fully charged stars, but this is not the case. This extra stretching of the inner part of the star can be due to pulling of the ends of the star branches, which are charged.

Furthermore, our calculations show that at the periphery of the star corona the effect of curvature on the conformations of the star branches is less important; i.e., the outermost regions of the star corona behave similarly as a planar annealed polyelectrolyte brush. This conclusion is supported by (i) a bimodal distribution of the end segments and (ii) a quasi-linear dependence of $\log(1 - \alpha)$ on z^2.

The evolution of the form factor of a star as a function of the salt concentration is totally different for a quenched and an annealed star. With decreasing the salt concentration the quenched star shows always oscillations, pronounced minima, and an increase in the slope of the initial decay of the form factor. In contrast, for annealed stars the oscillations and the minima dissappear with decreasing the salt concentrations, and the slope of the initial decay gets weaker.

The form factors calculated from numerical volume fraction profiles can be well-mapped to the experimental form factors measured by Groenewegen et al.[16] for annealing star-shaped polyelectrolyte micelles. Only the volume fraction profile in the annealing osmotic regime (with a decay of $z^{-8/3}$) is hard to fit to a one-power-law decay. This is due to the interference of a slower decay in the inner part of the star.

From this study, we got a detailed and consistent picture of the behavior of annealed and quenched polyelectrolyte stars. Furthermore, we have demonstrated that the numerical method we used is flexible and can mimick well experimental systems.

Acknowledgment. We acknowledge fruitful discussions with F. A. M. Leermakers. E.B.Z. acknowledges financial support from the National Science Foundation (Grant DMR-9973300). This work has been partially supported by the Dutch National Science Foundation (NWO) program "Self-Organization and Structure of Bionanocomposits" No. 047.009.016.

Appendix A. Dependence of a Reaction Constant on the Discretization

The reaction constant K used in the SCF calculation is dimensionless. So in principle, it should not depend on the lattice and in particular not on the thickness of the layers. For systems with only uncharged species it is indeed independent. For systems with charges, this is not the case because the thickness of the layer is determining the electrical capacitance of a layer, and with that the electrostatic potential decay.

Let us take the simple reaction of the dissociation of water:

$$2H_2O \leftrightarrows H_3O^+ + OH^- \tag{39}$$

The dissociation constant K_w used in practice is 10^{-14} mol^2 L^{-2} at room temperature and defined as

$$K_w \equiv [H_3O^+][OH^-] = 10^{-14}\ \text{mol}^2\,\text{L}^{-2} \tag{40}$$

where the square brackets denote the concentration in solution. To make K_w dimensionless, it has to be divided by the concentration of water squared, $[H_2O]^2$. The concentration of water in water is 55 mol L^{-1}; the value of the dissociation constant then becomes 3.3×10^{-18}. This value is correct if one uses a lattice based on the size of water, i.e., for a cubical lattice with the distance between two layers is 0.3 nm:

$$55\ \text{mol/L} = 55N_{av} \times 10^3\ \text{molecules/m}^3$$
$$= 33\ \text{molecules/nm}^3$$
$$a = \sqrt[3]{\frac{1}{33}}\ \text{nm} = 0.3\ \text{nm}$$

The conversion factor A in eq 38 is in this case 55 mol/L.

But instead of taking the distance between two layers equal to 0.3 nm, another value can be taken, for instance, the Bjerrum length or the Kuhn length of the polymer studied. In this case the dissociation constant should be normalized differently. The general idea is that the number of charges per volume should remain the same, because the Debye screening length should be indifferent to the distance between two layers. But due to different distances between the layers, the number of solvent molecules in a liter changes and therefore the K_w (actually, any reaction constant which includes the solvent molecules in the reaction).

As an example, we calculate the dissociation constant of water if the lattice size is taken to be the Bjerrum length l_B. The number of solvent molecules per liter decreases with a factor of $(l_B/0.3\ \text{nm})^3$; so instead of 55 mol/L, there are $55/(l_B/0.3\ \text{nm})^3$ solvent molecules in mol/L. The dissociation constant for water then becomes

$$K_w = \frac{10^{-14}}{\left(55/\left(\frac{l_B}{0.3\ \text{nm}}\right)^3\right)^2} \tag{41a}$$

$$= \frac{10^{-14}\left(\frac{l_B}{0.3\ \text{nm}}\right)^6}{55^2} \tag{41b}$$

So the conversion factor A in eq 38 from volume fractions to mol/L is, in the case when the thickness of the lattice layers is l_B, given by $55/(l_B/0.3\ \text{nm})^3$ mol/L.

Appendix B. Calculation of the Charge Distribution Fraction

The distribution function for the number n of dissociated segments in one branch is calculated by employing a modified propagator to the field given by the SCF solution. The end-segment weighting factor in eq 29 is split up according to the number of dissociated segments in the chain

$$G_n(z,s|1) = \alpha_{b,k=0}(s)G_{k=0}(z,s)\langle G_n(z,s-1|1)\rangle \quad (42a)$$

$$G_{n+1}(z,s|1) = \alpha_{b,k=-}(s)G_{k=-}(z,s)\langle G_n(z,s-1|1)\rangle \quad (42b)$$

where the subscript $k = 0$ denotes the neutral state of the segment and $k = -$ the charged state. The starting conditions of the new propagator read

$$G_0(z,1|1) = \alpha_{b,k=0}(1)G_{k=0}(z,1) \quad (43a)$$

$$G_1(z,1|1) = \alpha_{b,k=-}(1)G_{k=-}(z,1) \quad (43b)$$

To check whether the above given equations are calculated in the right way, the following equation must be true. The sum over all possible number of dissociated segments yields the total end-segment weighting factor:

$$\sum_n G_n(z,s|1) = G(z,s|1) \quad (44)$$

The distribution function $J(n)$ for the number n of dissociated segments can now be computed as

$$J(n) = \frac{\sum_z G_n(z,N|1)}{\sum_z G(z,N|1)} \quad (45)$$

References and Notes

(1) Kördel, W.; Dassenakis, M.; Lintelmann, J.; Padberg, S. *Pure Appl. Chem.* **1997**, *69*, 1571−1600.
(2) Torchilin, V. P. *J. Controlled Release* **2001**, *73*, 137−172.
(3) Borisov, O. V.; Daoud, M. *Macromolecules* **2001**, *34*, 8286−8293.
(4) Heinrich, M.; Rawiso, M.; Zilliox, J. G.; Lesieur, P.; Simon, J. P. *Eur. Phys. J. E* **2001**, *4*, 131−142.
(5) Ohshima, H. *J. Colloid Interface Sci.* **2000**, *228*, 190−193.
(6) Borisov, O. V. *J. Phys. II* **1996**, *6*, 1−19.
(7) Borisov, O. V.; Zhulina, E. B. *Eur. Phys. J. B* **1998**, *4*, 205−217.
(8) Klein Wolterink, J.; Leermakers, F. A. M.; Fleer, G. J.; Koopal, L. K.; Zhulina, E. B.; Borisov, O. V. *Macromolecules* **1999**, *32*, 2365−2377.
(9) Kiserow, D.; Prochazka, K.; Ramireddy, C.; Tuzar, Z.; Munk, P.; Webber, S. E. *Macromolecules* **1992**, *25*, 461−469.
(10) Khougaz, K.; Astafieva, I.; Eisenberg, A. *Macromolecules* **1995**, *28*, 7135−7147.
(11) Guenoun, P.; Delsanti, M.; Gazeau, D.; Mays, J.; Cook, D.; Tirrell, M.; Auvray, L. *Eur. Phys. J. B* **1998**, *1*, 77−86.
(12) Guenoun, P.; Davis, H. T.; Tirrell, M.; Mays, J. W. *Macromolecules* **1996**, *29*, 3965−3969.
(13) Guenoun, P.; Muller, F.; Delsanti, M.; Auvray, L.; Chen, Y. J.; Mays, J. W.; Tirrell, M. *Phys. Rev. Lett.* **1998**, *81*, 3872−3875.
(14) Förster, S.; Hemsdorf, N.; Leube, W.; Schnablegger, H.; Regenbrecht, M.; Akari, S.; Lindner, P.; Böttcher, C. *J. Phys. Chem. B* **1999**, *103*, 6657−6668.
(15) Muller, F.; Delsanti, M.; Auvray, L.; Yang, J.; Chen, Y. J.; Mays, J. W.; Demé, B.; Tirrell, M.; Guenoun, P. *Eur. Phys. J. E* **2000**, *3*, 45−53.
(16) Groenewegen, W.; Egelhaaf, S. U.; Lapp, A.; van der Maarel, J. R. C. *Macromolecules* **2000**, *33*, 3283−3293.
(17) Groenewegen, W.; Lapp, A.; Egelhaalf, S. U.; van der Maarel, J. R. C. *Macromolecules* **2000**, *33*, 4080−4086.
(18) Scheutjens, J. M. H. M.; Fleer, G. J. *J. Phys. Chem.* **1979**, *83*, 1619−1635.
(19) Atkins, P. W. *Physical Chemistry*; Oxford University: Oxford, 1998.
(20) Daoud, M.; Cotton, J. P. *J. Phys.* (*Paris*) **1982**, *43*, 531−538.
(21) Zhulina, E. B. *Polym. Sci. USSR A* **1984**, *26*, 794−798; *Vysokomol. Soedin., Ser. A.*
(22) Birshtein, T. M.; Zhulina, E. B. *Polymer* **1984**, *25*, 1453−1461.
(23) Currie, E. P. K.; Sieval, A. B.; Fleer, G. J.; Cohen Stuart, M. A. *Langmuir* **2000**, *16*, 8324−8333.
(24) Lyatskaya, Y. V.; Leermakers, F. A. M.; Fleer, G. J.; Zhulina, E. B.; Birshtein, T. M. *Macromolecules* **1995**, *28*, 3562−3569.
(25) Zhulina, E. B.; Birshtein, T. M.; Borisov, O. V. *Macromolecules* **1995**, *28*, 1491−1499.
(26) Zhulina, E. B.; Borisov, O. V. *Macromolecules* **1996**, *29*, 2618−2626.
(27) Fleer, G. J.; Cohen Stuart, M. A.; Scheutjens, J. M. H. M.; Cosgrove, T.; Vincent, B. *Polymers at Interfaces*; Chapman & Hall: London, 1993.
(28) Israëls, R.; Leermakers, F. A. M.; Fleer, G. J. *Macromolecules* **1994**, *27*, 3087−3093.
(29) van Male, J.; Leermakers, F. A. M.; Fleer, G. J., submitted to *J. Chem. Phys.*
(30) van Male, J.; Leermakers, F. A. M. "sfbox", 2001 A Computer Program.
(31) Wijmans, C. M.; Zhulina, E. B. *Macromolecules* **1993**, *26*, 7214−7224.
(32) Higgins, J. S.; Benoît, H. C. *Polymers and Neutron Scattering*; Oxford University Press: Oxford, 1994; Vol. 8.
(33) Press, W. H.; Teukolsky, S. A.; Vetterling, W. T.; Flannery, B. P. *Numerical Recipes in C, the art of scientific computing*, 2nd ed.; Cambridge University Press: Cambridge, 1992.
(34) Zhulina, E. B.; Klein Wolterink, J.; Borisov, O. V. *Macromolecules* **2000**, *33*, 4945−4953.
(35) Zhulina, E. B.; Borisov, O. V. *J. Chem. Phys.* **1997**, *107*, 5952−5967.
(36) Guo, X.; Ballauff, M. *Phys. Rev. E* **2001**, *64*, 015406.
(37) Guo, X. Synthesis and Study of the Colloidal Polyelectrolyte Brushes prepared by Photo-emulsion Polymerization. Thesis, University of Karlsrühe, 2001.

MA020781J